https://doi.org/10.48048/tis.2023.6099

Study of Diverse Leg Geometry Effect on the Performance of Segmented Thermoelectric Generator with the Same Leg Volume

Alkhadher Khalil[1,*], Ahmed Elhassnaoui[2], Said Yadir[3], Obbadi Abdellatif[1], Youssef Errami[1] and Smail Sahnoun[1]

[1]Laboratory Electronics, Instrumentation and Energy, Faculty of Sciences, ChouaïbDoukkali University, El Jadida 24000, Morocco
[2]National School of Applied Sciences - ENSABM, Sultan MoulaySlimane University, BeniMallal 23000, Morocco
[3]Laboratory of Materials, Processes, Environment and Quality, ENSA, Cadi Ayyad University, Safi 40000, Morocco

([*]Corresponding author's e-mail: alkhadher.k@ucd.ac.ma)

Received: 26 September 2022, Revised: 29 October 2022, Accepted: 5 November 2022, Published: 15 August 2023

Abstract

When developing any product, one of the factors that determine its price is the volume of the product. In this paper, the effect of various geometrical forms on the performance of a segmented TEGs with the same leg volume was performed. For this purpose, a numerical study was performed using the finite element method (FEM) for different geometrical shapes by considering 3 following forms: Rectangular-leg, Pin-leg, and Cone-leg. In each region, Bismuth Telluride was deposited on the cold side while Lead Telluride was placed on the hot side. Two cases were studied. In the 1st case, the 2 regions' the same length, for n and p types, which constitute the leg was taken. While in the 2nd case, all forms of the same volume were evaluated by taking a variable leg length and a fixed cross-sectional area of the hot side. The optimal ratios of the Bismuth Telluride lengths in $p_2 -$ type and $n_2 -$ type regions for the Rect-leg, Pin-leg, and Cone-leg were studied. The obtained results showed that the Rectangular-leg model in the 1st case presents the highest output power and efficiency with about 0.3019 watt and 12.47 % with leg length values of ($p_2 -$ type and$n_2 -$ type) 1 and 4.5 mm, respectively. Based on the simulation results, we conclude that the leg form and the length ratio influence the performance of the segmented TEGs. The findings indicate that the Rect-leg model presents the best performance.

Keywords: Segmented thermoelectric generator, Variable leg geometry, Same leg volume, Length ratio, Power, Efficiency, Performance

Introduction

Renewable energies are energy sources whose natural renewals are fast enough to be considered as inexhaustible on the human time scale. Overall, renewable energies are cleaner than fossil fuels and are currently used worldwide. They are more ecological, abundantly available around the globe, and are free of charge once production installations pay for themselves. The exploitation of these types of energy requires a system of conversion into useful energy. A TEG converts thermal into electricity. This generator is serene, without moving parts, very reliable, and environmentally friendly.

Thermoelectric generators made from skutterudite operate in the temperature range of 30 to 600 °C. Those made from Bismuth Telluride (Bi_2Te_3) operate in a range of 30 to 250 °C. Thermoelectric properties of the $Sn_{(1-x)}Bi_xTe$ were enhanced at high temperature from 300 to 1,000 K by Muthumari *et al.* [1]. Many studies have been performed to improve TEG efficiency. Numerical simulation of a hybrid system composed of concentrated CPV-TEG was performed to study efficiency with changing the solar radiation and module temperature by Mahmoudinezhad *et al.* [2]. The leg geometry effect is one of the studies carried out to improve segmented TEG efficiency using Bismuth Telluride and Lead Telluride. The results showed that by increasing the Pin form factor, the efficiency of the device is improved by Ali and Yilbas [3]. Maduabuchi [4], Modeling of TEG with X-leg geometry configuration to optimize the performance using high-temperature materials taking into consideration external load resistance, the taper angle of the X-leg, and the concentration ratio of the solar. The legs of thermocouples of TEG modules for 6 different models were studied. Results show that variable leg geometries effects temperature and voltage distributions were obtained by Maduabuchi *et al.* [5]. Maduabuchi *et al.* [6], Evaluation and comparison of the performance

of the solar thermoelectric generator of the Rectangular-leg and X-leg under the same operating conditions. The X-leg model presented higher temperature gradient, power output density and the efficiency compared to the Rectangular-leg. A simulation model of the segmented TEG for Rectangular-leg, trapezoidal-leg, and inverse trapezoidal-leg with different cross-sectional areas was analyzed using the finite element method. The trapezoidal-leg presents improvement in cooling of about 4.75 % by Ruiz-Ortega *et al.* [7]. A theoretical study of a solar thermoelectric system consisting of the thermocouple, the flat-panel selective solar absorber enclosed in an evacuated glass chamber and an optical concentrator. The results showed that the highest efficiency was obtained 5 %. In the case of hybrid photovoltaic-thermoelectric systems (PV-TE), the highest output power is obtained when the area ratio of the 2 doped regions n-type and p-type is $A_n/A_p = 1$. Whereas the TEG system has the highest output power when $A_n/A_p < 1$ by Li *et al.* [8]. Shittu *et al.* [9], the results also showed that the PV cell characteristics affect the optimal PV-TE geometry. A study of the effect of the trapezoidal leg on the performance of the TEG by Raihan Mohammad Siddique *et al.* [10]. In addition, the trapezoidal-formed generated the highest temperature difference when the input current is 5A, and it was more than the Rectangular-formed about 10 % by Siddique *et al.* [11]. Shittu *et al.* [12], the performance of the hybrid system PV-TE can be improved using an optimized thermoelectric geometry. Ibeagwu [13], the study and evaluation of the TEGs with diverse variable legs were performed. The comparative study by numerical modeling of the performance of TEG using the leg's same volume with diverse geometries showed that the Rectangular leg presented the best performance by Khalil *et al.* [14]. Numerical performance evaluation of 3 TEG leg geometries showed that a Diamond-leg encountered lower thermal stresses and generated a larger voltage difference than the Rectangular and Cone-leg models design Doraghi *et al.* [15]. Al-Merbati *et al.* [16] the study of the surface ratio effect R_A of the hot junction A_H compared to the cold junction A_L showed an improvement in thermal efficiency and a decrease in heat stress for $R_A \leq 0.5$ and $R_A \geq 2$.

Segmented thermoelectric generators represent an important area of research to enhance the performance of thermoelectric devices and extend the operating temperature ranges. Ruiz-Ortega *et al.* [17] Behavior of the segmented thermoelectric generator (STEG) with a variable heat input power on the hot side was studied. While the heat on the cold side is losing by natural convection. Design [18], Compare the performance of TEGs was performed, with a rectangular leg, segmented leg, and a variable cross-sectional leg to optimize the performance of TEG. The results showed that segmented TEG presented output power the highest than traditional TEG of about 51.71 %. The influences of the Thomson and the segmented leg geometry on the cooling power (Q_C) and coefficient of performance (COP) of a segmented TEG cooler were evaluated. The results showed that the STEMC system was found to deliver a maximum cooling power that was 5.10 % higher than that of the traditional TEMC by Badillo-Ruiz *et al.* [19]. Kumar *et al.* [20] a numerical study of a thermoelectric generator of a pin leg was carried out using ANSYS software. The study depends on the improvement of the solar concentration ratio, convective film coefficient, leg length and area.

Tian *et al.* [21], Comparison of output performance obtained using segmented and conventional TEGs with external resistance at heat source temperatures ranging from 500 to 800 K showed that segmented TEGs exhibited the best performance with 1.55 W output power and efficiency at 9.6 %. Liu *et al.* [22], a segmented STEG with an asymmetric leg can generate 4.21 % more power output than symmetric legs. The length ratio effect analysis of the segmented TEG on the output performance showed that there is an optimal length ratio generating the highest output power and efficiency by Zhang *et al.* [23]. Tian *et al.* [24], the segmented TEG performance and traditional TEG were compared based on the hot of exhaust gas (DE) and cold source temperature, length and cross-section area, and heat transfer coefficient. The optimal segmented TEGs were studied with minimal semiconductor volume. The results showed that the optimal segmented TEGs give the best performance compared to the skutterudite TEG module with an increase in the percentages of the highest output power and efficiency by Ge *et al.* [25]. Best performance of segmented TEGs is obtained with an optimal ratio of 25 % bismuth telluride and 75 % skutterudite for the p-leg and n-leg by Shittu *et al.* [26]. Shittu *et al.* [27] 3-dimensional numerical analysis using the finite element method demonstrated that the segmented annular TEG (SATEG) has a higher performance than the annular TEG (ATEG). When $\Delta T = 200K$, the SATEG presenters the efficiency highest Compared to ATEG for Bismuth telluride and Skutterudite.

The aim of this study is to evaluate the effects of cross-sectional area, leg length, and length ratios on the performance of segmented TEGs using 3 equal-volume forms: Recto-leg, Pin-leg, and Cone-leg. The performance comparison of segmented thermoelectric generators (TEGs) and traditional TEG using studied legs is also evaluated.

Nomenclature

A	Cross sectional area (m²)	T_C	Cold side temperature (K)
A_{int}	Interface area (m²)	T_H	Hot side temperature (K)
I	Current (A)	T_{int}	Temperature of interface area (K)
V	Voltage (V)	K_{TH}	Thermal conductance of model (W/K)
v_{leg}	Thermoelectric leg volume (m^3)	ΔT_{TH}	Temperature difference (K)
L	Leg length (m)	η	Efficiency (%)
p	Output power (W)	k_{n}	Thermal conductivity (n-type) (W/m.k)
Q_C	Heat flow at the cold side (W)	k_{p}	Thermal conductivity (p-type) (W/m.k)
Q_H	Heat flow at the hot side (W)	μ	Thomson coefficient (V/K²)
R	Electrical resistance (ohm)	σ_n	Electrical conductivity (n-type) (S/m)
R_G	Total electrical resistance (ohm)	σ_p	Electrical conductivity (p-type) (S/m)
R_L	External load resistance (ohm)		
R_{TH}	Thermal electrical resistance (ohm)		
α_n	Seebeck coefficient (n-type) (V/K)		
α_p	Seebeck coefficient (p-type) (V/K)		

Description of the studied models

In this study, the segmented thermocouples (TEGs) are modeled and simulated for 3 different geometrical forms Rect-leg, Pin-leg, and Cone-leg in 2 cases: In the 1st case, all forms have the same length and volume. In the 2nd case, the same volume and the hot side area, as shown in **Figure 1** and **Figure 2**.

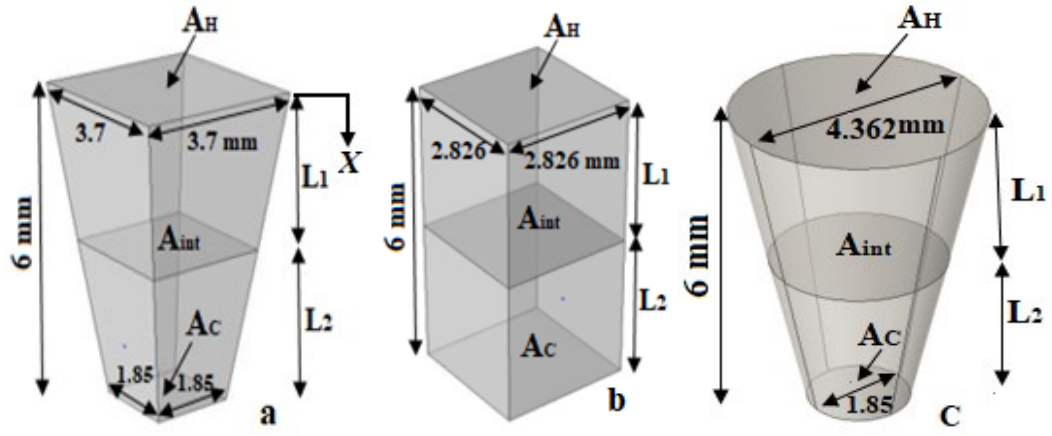

Figure 1 (a) Pin-leg, (b) Rect-leg, and (c) Cone-leg (1st case).

The Pin-leg volume calculate by Eq. (1);

$$v_{Pin-leg} = \left[\frac{1}{3}L\left(A_H + A_C + \sqrt{A_H.A_C}\right)\right] = 47.915 * 10^{-9}\, m^3 \quad (1)$$

$$v_{Rect-leg} = v_{Cone-leg} = v_{Pin-leg} = 47.915 * 10^{-9}\, m^3 \quad (2)$$

$$L_{Rect-leg} = L_{Cone-leg} = L_{Pin-leg} = 6 * 10^{-3}\, m \quad (3)$$

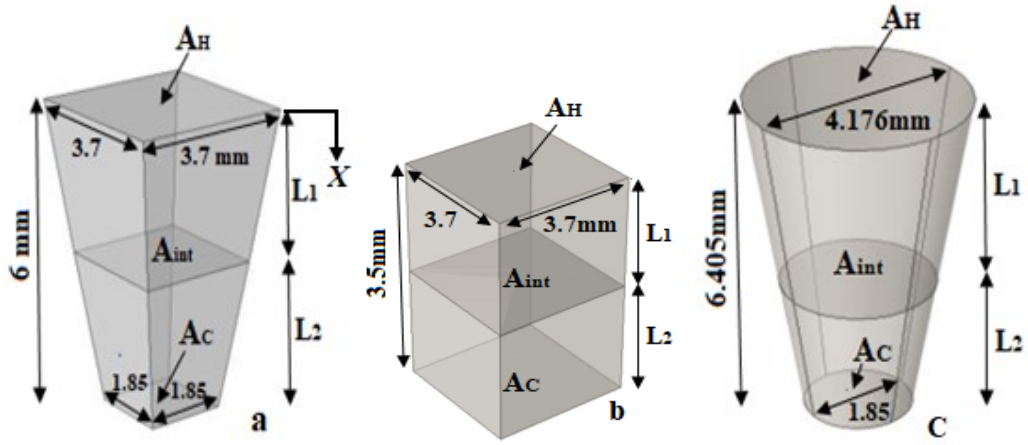

Figure 2 (a) Pin-leg, (b) Rect-leg, and (c) Cone-leg (2nd case).

$$A_{H,Rect-leg} = A_{H,Cone-leg} = A_{H,Pin-leg} = 13.69 * 10^{-6}\ m^2 \quad (4)$$

The length of Bismuth Telluride for $p_2 -$ type and $n_2 -$ type in the Rect-leg, Pin-leg, and Cone-leg shapes are changed to study its effect on performance and get an optimal length ratio.

Study of the segmented TEGs

In the TEGs, the conversion of thermal into electrical depends on the temperature difference between the hot and cold sides. The materials chosen to perform this work are those most commonly used in this type of study. Suzuki *et al.* [28], and Angelo *et al.* [29]. In the segmented TEGs, the materials with a low-temperature range are placed as the Bismuth Telluride on the cold side. While the materials with the high-temperature range as the modified Lead Telluride are deposited on the hot side. $\boldsymbol{\alpha}$, $\boldsymbol{\sigma}$, and $\boldsymbol{k}$ are functions of temperature, as show in **Table 1**.

Table 1 Properties of bismuth telluride and modified lead telluride [28,29].

Properties	$\boldsymbol{n_1 - type(Ag_{0.86}Pb_{19+x}SbTe_{20})}$	**Units**
$\alpha(T)$	$(173.26 - 3.8229 * T + 0.011679 * T^2 - 1.5584 * 10^{-5} * T^3 + 7.6695 * 10^{-9} * T^4) * 10^{-6}$	$(^{V}/_{K})$
$\sigma(T)$	$(1462 - 10.419 * T + 0.031315 * T^2 - 4.0429 * 10^{-5} * T^3 + 1.9034 * 10^{-8} * T^4) * 10^2$	$(^{S}/_{m})$
$k(T)$	$0.6586 + \frac{329.63}{T} + \frac{22145}{T^2}$	$(^{W}/_{m.K})$
Properties	$\boldsymbol{p_1 - type(Ag_{0.9}Pb_9Sn_9Sb_{0.6}Te_{20})}$	**Units**
$\alpha(T)$	$(52.884 - 0.24828 * T + 1.138 * 10^{-3} * T^2 - 7.6468 * 10^{-7} * T^3) * 10^{-6}$	$(^{V}/_{K})$
$\sigma(T)$	$(179.02 + 12.336 * T - 0.042167 * T^2 + 5.129 * 10^{-5} * T^3 - 2.1435 * 10^{-8} * T^4) * 10^2$	$(^{S}/_{m})$
$k(T)$	$0.56959 + \frac{550.66}{T} - \frac{47483}{T^2}$	$(^{W}/_{m.K})$
Properties	$\boldsymbol{n_2 - type(Bi_2Te_3)}$	**Units**
$\alpha(T)$	$(0.00153073 * T^2 - 1.08058874 * T - 28.338095) * 10^{-6}$	$(^{V}/_{K})$
$\sigma(T)$	$(0.01057143 * T^2 - 10.16048 * T + 3113.714229) * 10^2$	$(^{S}/_{m})$
$k(T)$	$0.0000334545 * T^2 - 0.023350303 * T + 5.606333$	$(^{W}/_{m.K})$
Properties	$\boldsymbol{p_2 - type(Bi_2Te_3)}$	**Units**
$\alpha(T)$	$(-0.003638095 * T^2 + 2.74380952 * T - 296.214286) * 10^{-6}$	$(^{V}/_{K})$
$\sigma(T)$	$(0.015601732 * T^2 - 15.708052 * T + 4466.38095) * 10^2$	$(^{S}/_{m})$
$k(T)$	$0.0000361558 * T^2 - 0.026351342 * T + 6.22162$	$(^{W}/_{m.K})$

Finite element method

A 3D simulation for a thermoelectric model system using FEM is built to solve the electric field and temperature equations;

$$\nabla(k\nabla T) + \rho \boldsymbol{J}^2 - TJ.\left[\left(\frac{\partial \alpha}{\partial T}\right)\nabla T + (\nabla \alpha)_T\right] = 0 \quad (5)$$

$$\nabla.\boldsymbol{J} = 0 \quad (6)$$

$$\boldsymbol{J} = -\sigma\left[\nabla\left(\frac{\mu}{e} + V\right) + \alpha\nabla T\right] \quad (7)$$

$$\boldsymbol{q} = \alpha T\boldsymbol{J} - k\nabla T \quad (8)$$

Figure 3 shows the flowchart of the stages of the simulation.

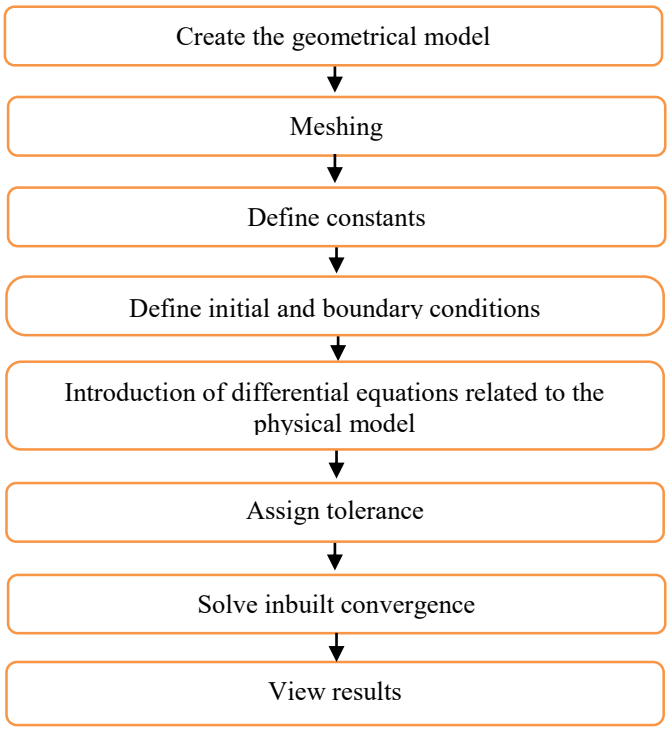

Figure 3 Flowchart of the simulation El-abidi *et al.* [30].

Boundary conditions

In this study, the different geometries are discretized into tetrahedral elements, as seen in **Figure 4(a) - 4(c)**. To facilitate the numerical solution some assumptions are considered in the simulation;

(1) The temperatures of the hot and cold ceramic junctions for all studied cases are equal to 700 and 300 K, respectively.

(2) Heat convection heat and heat radiation on all surfaces are neglected.

(3) Electrical contact resistance and thermal contact resistance are not considered.

(4) All other surfaces except the hot and cold surfaces are adiabatic.

(5) Assumed that a steady state is achieved and that the leg surfaces are isolated.

(6) No difference in properties as a function of position exist.

(7) The relative tolerance is fixed at 10^{-3}.

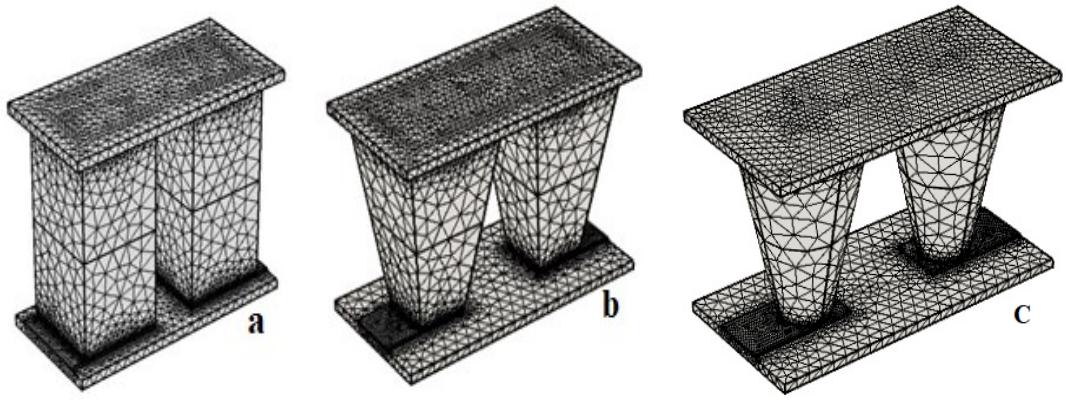

Figure 4 The models mesh type. (a) Rect-leg, (b). Pin-leg, and (c) Cone-leg.

Performance of segmented TEGs

The electrical output power generated by the segmented thermocouple depends on 4 physical concepts; $\boldsymbol{\alpha}$, $\boldsymbol{R_{TH}}$, $\boldsymbol{R_{th}}$, and $\Delta \boldsymbol{T}$. The $\boldsymbol{\sigma}$ $\boldsymbol{and}$ $\boldsymbol{k}$ values are evaluated at the average junction temperature. While for Seebeck coefficient an integral-averaged value is employed. The average $\boldsymbol{\alpha}$ of the p-leg and n-leg can be expressed by the following equations;

$$\alpha_P = \frac{1}{T_H - T_C}\left(\int_{T_{int}}^{T_H} \alpha_{p_1}(T)dT \ + \int_{T_H}^{T_{int}} \alpha_{p_2}(T)dT \ \right) \tag{9}$$

$$\alpha_n = \frac{1}{T_H - T_C}\left(\int_{T_{int}}^{T_H} \alpha_{n_1}(T)dT \ + \int_{T_H}^{T_{int}} \alpha_{n_2}(T)dT \ \right) \tag{10}$$

Where $\alpha = \alpha_p - \alpha_n$

Electrical and thermal resistance depends on leg dimensions and electrical and thermal conductivity. The electrical resistance of p-leg and n-leg were expressed in the following equations;

$$R_{\mathrm{p}} = \frac{1}{\sigma_1(T)}\int_0^{L_1}\frac{dx}{A(x)} + \frac{1}{\sigma_2(T)}\int_{L_1}^{L}\frac{dx}{A(x)} \tag{11}$$

$$R_n = \frac{1}{\sigma_1(T)}\int_0^{L_1}\frac{dx}{A(x)} + \frac{1}{\sigma_2(T)}\int_{L_1}^{L}\frac{dx}{A(x)} \tag{12}$$

The cross-sectional areas of the studied models are given as [13]:

$$A(0 \le x \le L)_{Rect-leg} = A_H = A_C \tag{13}$$

$$A(0 \le x \le L)_{Pin-leg} = \frac{A_H - A_C}{L}x + A_C \tag{14}$$

$$A(0 \le x \le L)_{Cone-leg} = \frac{A_H - A_C}{L}x + A_C \tag{15}$$

The internal resistance of Bismuth Telluride and modified Lead Telluride (p-n type) shown in **Figure 1** and **Figure 2** can be written by the Eqs. (16) - (18);

$$R_{Rect-leg} = \left(\frac{L_1}{A_H\sigma_1(T)} + \frac{L_2}{A_H\sigma_2(T)}\right) \tag{16}$$

$$R_{Pin-leg} = \left(\frac{1}{\sigma_1(T)}\right)\left\{\frac{L_1}{(A_H - A_{int})}ln\left(\frac{A_H}{A_{int}}\right)\right\} + \left(\frac{1}{\sigma_2(T)}\right)\left\{\frac{L_2}{(A_{int} - A_C)}ln\left(\frac{A_{int}}{A_C}\right)\right\} \tag{17}$$

$$R_{Cone-leg} = \left(\frac{L_1}{\sigma_1(T)}\right)\left\{\frac{1}{(A_H - A_{int})} ln\left(\frac{A_H}{A_{int}}\right)\right\} + \left(\frac{L_2}{\sigma_2(T)}\right)\left\{\frac{1}{(A_{int} - A_C)} ln\left(\frac{A_{int}}{A_C}\right)\right\} \quad (18)$$

The total internal resistance of p and n type can be given by the following equation;

$$R_{el} = R_{n,leg} + R_{pleg} = R_{n_1} + R_{n_2} + R_{p_1} + R_{p_2} \quad (19)$$

The thermal resistance of the Bismuth Telluride leg and the modified Lead Telluride of p and n type shown in **Figure 1** and **Figure 2** can be calculated by the Eqs. (20) - (22);

$$R_{th_{Rect-leg}} = \left(\frac{L_1}{A_H k_1(T)} + \frac{L_2}{A_H k_2(T)}\right) \quad (20)$$

$$R_{th_{Pin-leg}} = \left(\frac{1}{k_1(T)}\right)\left\{\frac{L_1}{(A_H - A_{int})} ln\left(\frac{A_H}{A_{int}}\right)\right\} + \left(\frac{1}{k_2(T)}\right)\left\{\frac{L_2}{(A_{int} - A_C)} ln\left(\frac{A_{int}}{A_C}\right)\right\} \quad (21)$$

$$R_{th_{Cone-leg}} = \left(\frac{L_1}{k_1(T)}\right)\left\{\frac{1}{(A_H - A_{int})} ln\left(\frac{A_H}{A_{int}}\right)\right\} + \left(\frac{L_2}{k_2(T)}\right)\left\{\frac{1}{(A_{int} - A_C)} ln\left(\frac{A_{int}}{A_C}\right)\right\} \quad (22)$$

Thermal conductance of p and n type can be given by the following equation;

$$K_{TH} = \frac{1}{R_{th_{n1}} + R_{th_{n2}}} + \frac{1}{R_{th_{p1}} + R_{th_{p2}}} \quad (23)$$

The heat of Q_H and the heat of Q_C can be expressed by Eqs. (24) - (25);

$$Q_H = [\alpha I T_H + K_{TH}\Delta T_{TE} - (0.5 * R_G I^2) - (0.5 * I\tau\Delta T_{TE})] \quad (24)$$

$$Q_C = [\alpha I T_C + K_{TH}\Delta T_{TE} + (0.5 * R_G I^2) + (0.5 * I\tau\Delta T_{TE})] \quad (25)$$

The current can be written by;

$$I = \frac{\alpha\Delta T_{TE}}{R_G + R_L} \quad (26)$$

Electrical output power can be calculated by Eqs. (24) - (25);

$$P = Q_H - Q_C = \alpha I\Delta T_{TE} - R_G I^2 \quad (27)$$

The efficiency can be expressed by the following equation;

$$\boldsymbol{\eta = \frac{P}{Q_H} = \frac{P}{\alpha I T_H + K_{TH}\Delta T_{TE} - (0.5 * R_G I^2) - (0.5 * I\tau\Delta T_{TE})}} \quad (28)$$

Results and discussion

Analysis of the geometric effect on the temperature distribution

In this study, numerical modeling of the segmented TEGs models of Rect-leg, Pin-leg, and Cone-leg were performed with the same leg volume when the shapes of hot and cold are in stable conditions at 700 and 300 K. The temperature distribution of thermoelectric materials depends on many basic parameters. One of these parameters is the geometrical form of the leg, where the leg geometry affects the path of the temperature with leg length. **Figure 5(a) - 5(b)** show temperature distribution for thermoelectric materials of p and n type with the leg length.

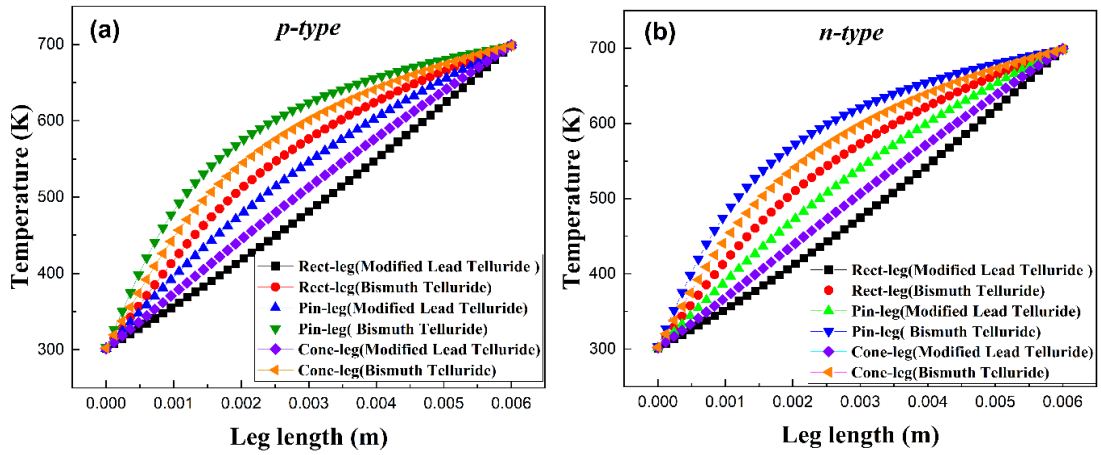

Figure 5 Variation of temperature with the traditional leg length; (a) p-type, (b) n-type.

Figure 6(a) - 6(b) show the values of the output power and the efficiency of the studied models in the 2 cases using the material of the modified Lead Telluride. In the 1st case, although the Rect-leg model had the smallest cross-sectional area for the hot side, it presented the best performance with output power and efficiency with values of 0.2247 W and 10.52 %, respectively. While, the Pin-leg model presented the lowest efficiency of about 10.39 %. For the 2nd case, a variable leg length significantly affects the performance of the Rect-leg model, where the Rect-leg presented the output power the higher than the Pin-leg and Cone-leg with about 68.5 and 72.8 %, respectively, and the Pin-leg presented the highest efficiency of 10.39 %, as shown in **Table 2**.

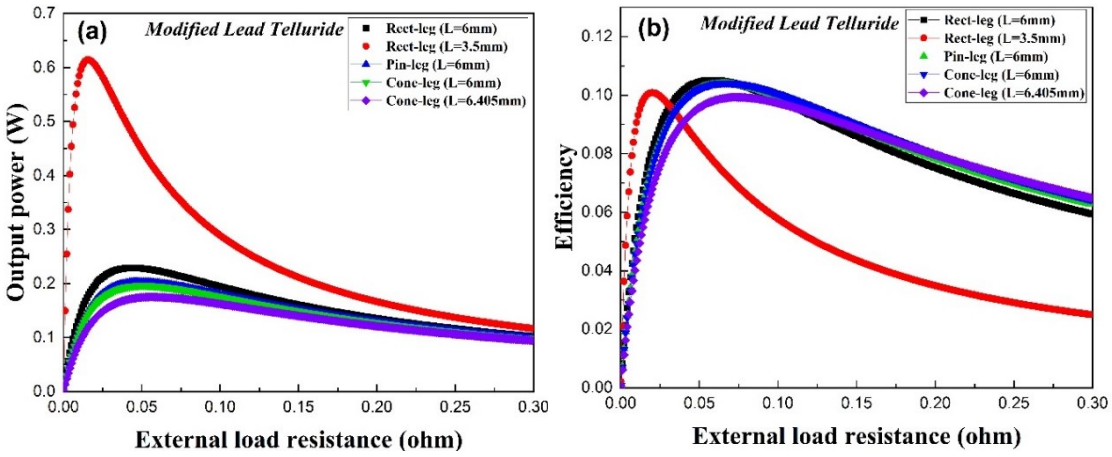

Figure 6 (a) output power, (b) Efficiency of the traditional TEG with external load resistance.

Table 2 Performance of traditional TEGs models.

Model	The same volume and leg length (1st case)		The same leg volume and cross-sectional area of the hot ceramic (2nd case)	
	Power (*P*) (W)	Efficiency (η_{max}) (%)	Power (*P*) (W)	Efficiency (η_{max}) (%)
Rect-leg	0.225	10.52	0.632	10.08
Pin-leg	0.199	10.39	0.199	10.39
Cone-leg	0.193	10.42	0.172	9.93

In addition, the effect of the changing leg geometry on the heat flow path through thermoelectric materials. Thermal properties such as thermal conductivity affect the flow path. For the segmented TEGs, in the area between the 2 materials, a sudden change in the heat flow path occurs. **Figure 7(a) - 7(b)** show the paths of heat flow through the segmented leg of p and n type. $\boldsymbol{\alpha}$, $\boldsymbol{\sigma}$, and $\boldsymbol{k}$ of the p and n type are

calculated using temperature distributions between the cold side and the interface area. For the modified Lead Telluride is calculated using the temperature distributions between the hot side and the interface area.

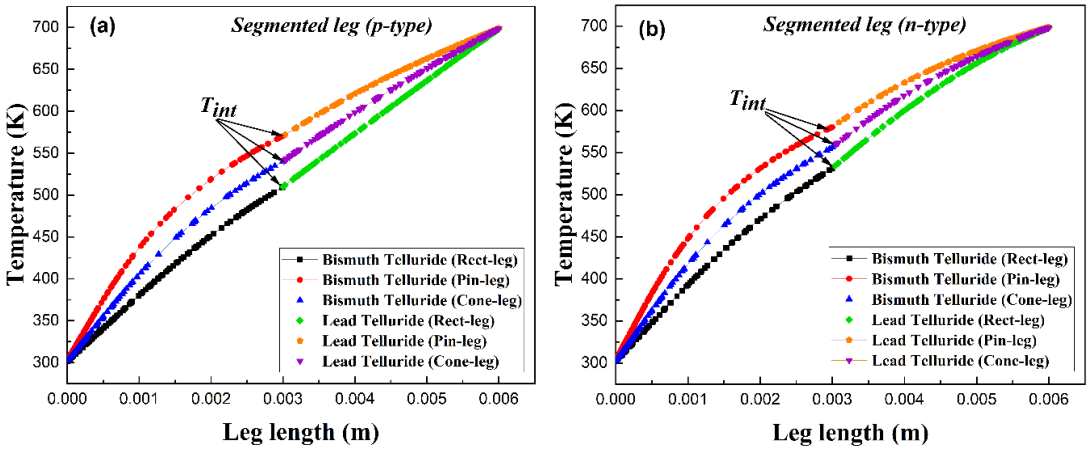

Figure 7 Variation of temperature with the segmented leg length; (a). Rect-leg, (b). Pin-leg and Cone-leg.

Figure 8(a) presents the temperature of the interface area between thermoelectric materials for the Lead Telluride and Bismuth Telluride of n and p-type with the leg length for the studied shapes in the 1st case. While **Figure 8(b)** shows the temperature of the interface area of the 2nd case. The temperature of the interface area varies for the leg shape and length ratio.

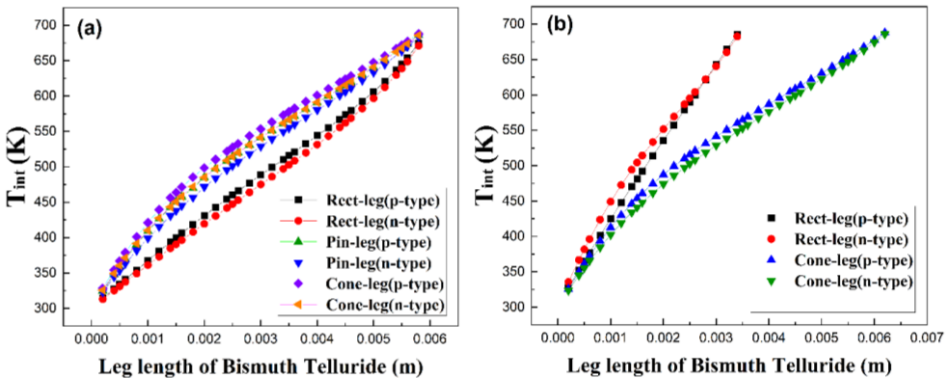

Figure 8 Variation of interface temperature with leg length; (a) 1st case, (b) 2nd case.

Performance analysis of the segmented TEGs

Although all forms of the segmented thermocouple in the 1st case have the same volume and leg length, the variable cross-sectional area affects the electrical resistance and thermal conductivity values. **Figure 9(a)** shows that the Rect-leg has the lowest electrical resistance, and the Cone-leg gives the highest value, while the Cone-leg gives the lowest thermal conductance, as shown in **Figure 9(b)**. In the 2nd case, although all forms have the same hot ceramic junction area, the variable leg length generates significant changes in the electrical resistance and thermal conductance for the Rect-leg, as shown in **Figure 10(a)** - **10(b)**.

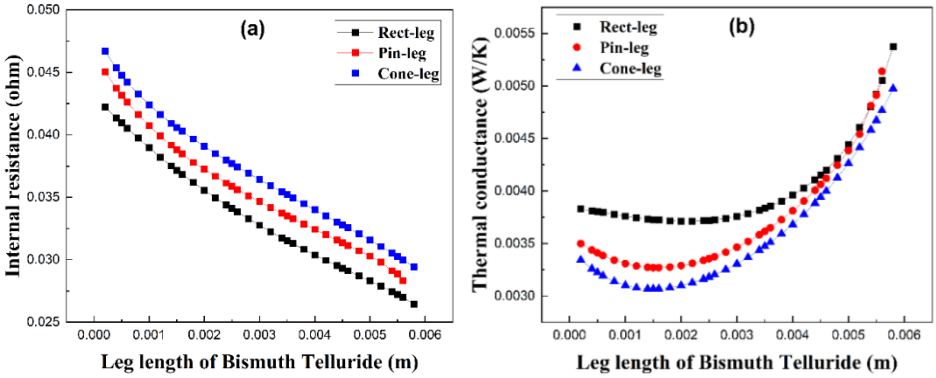

Figure 9 (a) internal resistance, (b) Thermal conductance (1st case).

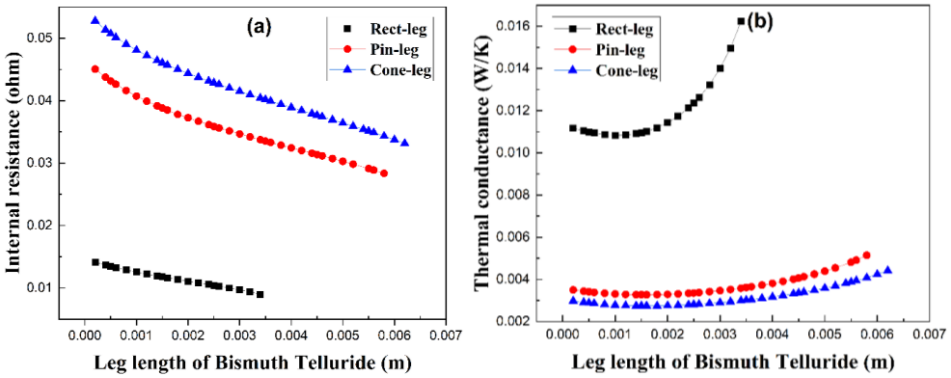

Figure 10 (a) internal resistance, (b) Thermal conductance (2nd case).

The performance of segmented TEGs is affected by the thermoelectric leg geometry and length ratio. **Figure 11(a) - 11(f)** and **Figure 12(a) - 12(d)** present the efficiency and output power with a leg length of Bismuth Telluride of $p_2 -$ type and $n_2 -$ type for the studied models in the 2 cases when the ratio between the internal and the external resistance is$(R_G/R_l = 1)$.

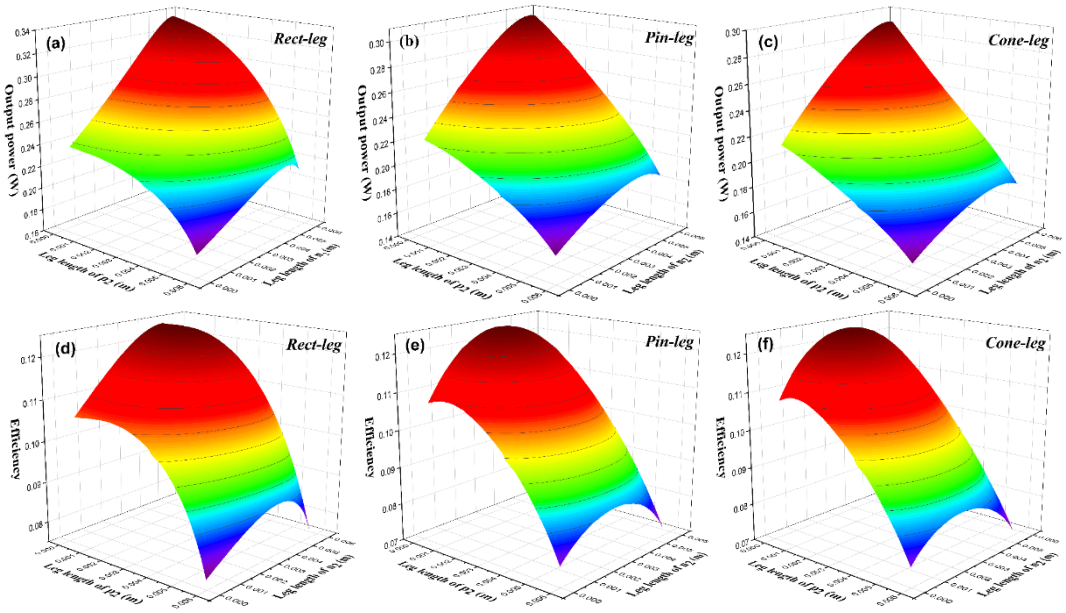

Figure 11 (a-c) Output power, (d-f) Efficiency of Rect-leg, Pin-leg, and Cone-leg with leg length of Bismuth Telluride for$p_2 - type\ and\ n_2 - type$ (1st case).

The Rect-leg generates the highest efficiency and output power with the leg length of Bismuth Telluride for p_2- type and n_2- type 1 and 4.5 mm, as shown in **Figure 11(a)** - **11(d)**. While the Cone-leg generates the lowest output power with the leg length of Bismuth Telluride for p_2- type and n_2- type 0.8 and 4 mm (**Figure 11(c)**), and the Pin-leg has the lowest efficiency when 0.6 and 3.6 mm, respectively (**Figure 11(e)**).

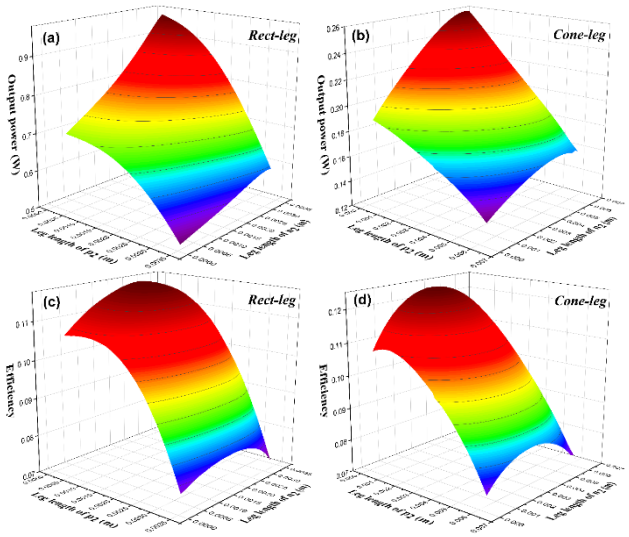

Figure 12 (a-c) Output power, (d-f) Efficiency of Rect-leg and Cone-leg with leg length of Bismuth Telluride for$p_2-type\ and\ n_2-type$ (2nd case).

The variable leg length (2nd case) has a significant impact on the performance. The Rect-leg gives the lowest efficiency and highest output power with the leg length of Bismuth Telluride for p_2- type and n_2- type 0.4 and 2.6 mm, as shown in **Figure 12(a)** - **12(c)**. While, the Cone-leg model presents the highest efficiency when 0.6 and 3.6 mm, respectively, as shown in **Figure 12(d)**. **Table 3** shows the optimum length of $p_1, p_2\ and\ n_1, n_2-type$ for the studied models in the 2 cases. The optimal length ratios vary from one form to another. This is due to the effect of effective area and variable leg length.

Table 3 Optimum leg length for the thermoelectric materials used of $p-$ type and $n-$ type.

Model	1st case				2nd case			
	L_{P_1}	L_{P_2}	L_{n_1}	L_{n_2}	L_{P_1}	L_{P_2}	L_{n_1}	L_{n_2}
Rect-leg	0.005	0.001	0.0015	0.0045	0.0031	0.0004	0.0009	0.0026
Pin-leg	0.0054	0.0006	0.0024	0.0036	0.0054	0.0006	0.0024	0.0036
Cone-leg	0.0052	0.0008	0.002	0.004	0.005805	0.0006	0.002805	0.0036

The Rect-leg model in the 2 cases has the highest effective area. Therefore, it generates the value highest output power. **Figure 13** and **Figure 14** show the efficiency and output power of the studied models with the optimal ratios shown in **Table 3**.

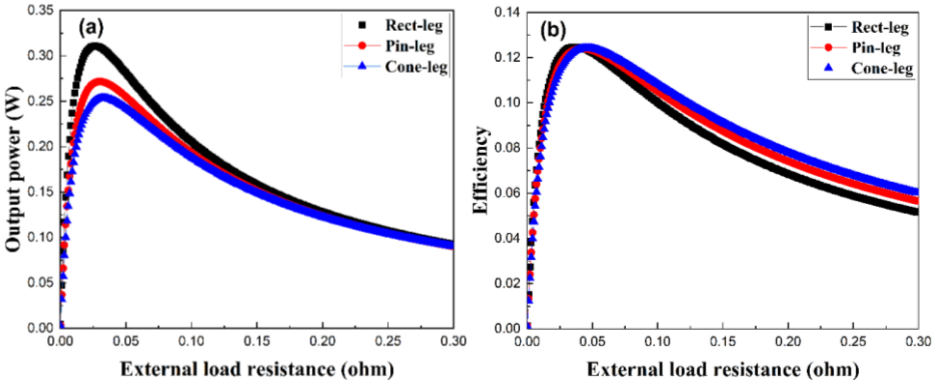

Figure 13 (a) output power, (b) Efficiency (1st case).

The Rect-leg model (1st case) presented the best performance with efficiency and output power of about 12.47 %, 0.302 W, While the Pin-leg presented 12.40, 0.264 W, and the Cone-leg 12.42 %, 0.246 W, as shown in **Figure 13(a) - 13(b)**. The 2nd case shows that the Rect-leg generates the highest output power and the lowest efficiency of 0.814 W, 11.71 %, where its output power is highest than the Pin-leg and Cone-leg with about 67.6 and 72.6 %. While, the Cone-leg generates the highest efficiency and lowest output power of about 12.45 %, 0.223 W, as shown in **Figure 14(a) - 14(b)** and **Table 4**.

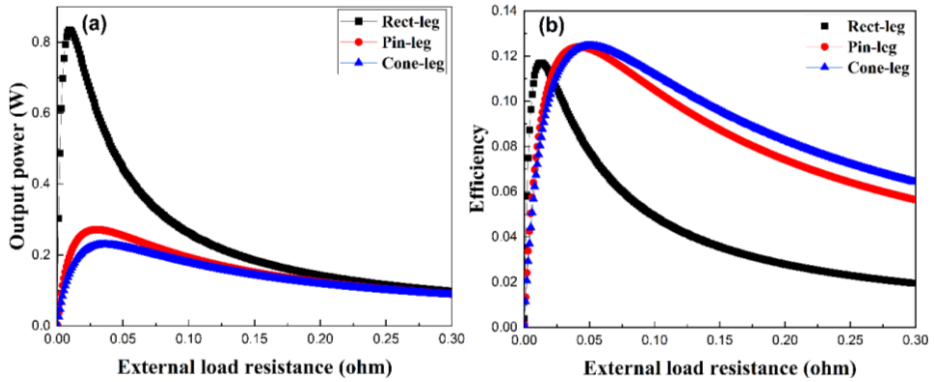

Figure 14 (a) output power (b) Efficiency (2nd case). The segmented Rect-leg model in the 1st case presented the best performance.

Table 4 Performance of segmented TEGs models.

Model	(1st case)		(2nd case)	
	Power (*P*) (W)	**Efficiency (η_{max}) (%)**	**Power (*P*) (W)**	**Efficiency (η_{max}) (%)**
Rect-leg	0.302	12.47	0.814	11.71
Pin-leg	0.264	12.40	0.264	12.40
Cone-leg	0.246	12.42	0.223	12.45

Conclusions

A numerical study of traditional and segmented thermocouples of Rect-leg, Pin-leg, and Cone-leg forms having the same volume was performed. In the segmented TEG, the modified Lead Telluride with the high-temperature range is deposited on the hot side, and Bismuth Telluride with the low-temperature range is placed on the cold side. The effects of cross-sectional area, leg length, and length ratios on the performance segmented TEGs were evaluate taking consideration the properties of thermoelectric materials that depend on temperature. The hot and cold are at 700 and 300 K. The results are summarized in the following points;

The temperature distribution of the segmented TEGs leg depends on the effective area and the thermal properties.

The interface area temperature varies with the variable leg geometry and length ratios of the materials used, and its increase affects the efficiency of the segmented thermocouple when it is above the Bismuth Telluride optimum temperature range.

The leg geometry and the length ratios of the Bismuth Telluride of n and p-type affect the electrical and thermal resistance.

By considering different legs with same lengths and volume, in the case of traditional TEG model the rectangular leg model produced the best performance of 10.52 %. While, in the case of segmented TEG, the Rect-leg model provided the best output power and efficiency of 0.302 W and 12.47 %, respectively.

By considering different legs with same cross-sectional area and volume, the Rect-leg produced the highest output power and the lowest efficiency of about 0.814 W and 11.71 %, respectively. While, the Cone-leg provided the highest efficiency and the lowest output power of about 12.45 % and 0.223 W, respectively.

The results show that the segmented TEG for the Recto-leg, Pin-leg and Cone-leg has a better efficiency compared to traditional TEG models.

In all cases and by considering the same leg volume and varying forms, the rectangular leg model provides the best performance compared to the other models.

Volume is considered an essential factor in manufacturing. Therefore, the same leg volume is given for the studied shapes. Based on the results of the numerical study in this work, it was found that the segmented thermoelectric generator is the best compared to the traditional generator. Therefore, the results of this study can be used in the design of thermoelectric generators to improve performance. Our future directions are to conduct experimental studies of the different geometric shapes of the segmented thermoelectric generator with the same leg volume to get the best performance at a lower cost.

The volume of a TEG is considered a key factor in manufacturing and the results of its study can serve to design and realize low-cost TEGs.

References

[1] M Muthumari, M Manjula, K Pradheepa, M Maaza and P Veluswamy. Revealing enhanced thermoelectric performance of tin-bismuth-telluride materials. *Bull. Mater. Sci.* 2022; **45**, 167.

[2] S Mahmoudinezhad, A Rezania and LA Rosendahl. Behavior of hybrid concentrated photovoltaic-thermoelectric generator under variable solar radiation. *Energ. Convers. Manag.* 2017; **164**, 443-52.

[3] H Ali and BS Yilbas. Innovative design of a thermoelectric generator of extended legs with tapering and segmented pin configuration: Thermal performance analysis. *Appl. Therm. Eng.* 2017; **123**, 74-91.

[4] CC Maduabuchi, MN Eke and CA Mgbemene. Solar power generation using a two-stage X-leg thermoelectric generator with high-temperature materials. *Int. J. Energ. Res.* 2021; **45**, 13163-81.

[5] C Maduabuchi, K Ejenakevwe, A Ndukwe and C Mgbemene. High performance solar thermoelectric generator using asymmetrical variable leg geometries. *E3S Web Conferences* 2021; **239**, 00005.

[6] C Maduabuchi, KA Ejenakevwe, I Jacobs, N Agwu and C Mgbemene. Analysis of a two-stage variable leg geometry solar thermoelectric generator. *In*: Proceedings of the 2nd African International Conference on Industrial Engineering and Operations Management, Harare, Zimbabwe. 2021.

[7] PE Ruiz-Ortega, MA Olivares-Robles and CA Badillo-Ruiz. Transient thermal behavior of a segmented thermoelectric cooler with variable cross-sectional areas. *Int. J. Energ. Res.* 2021; **45**, 19215-25.

[8] G Li, X Zhao, YI Jin, X Chen, JIE Ji and S Shittu. Performance analysis and discussion on the thermoelectric element footprint for PV - TE maximum power generation. *J. Electron. Mater.* 2018; **47**, 5344-51.

[9] S Shittu, G Li, X Zhao and X Ma. Series of detail comparison and optimization of thermoelectric element geometry considering the PV effect. *Renew. Energ.* 2019; **130**, 930-42.
[10] ARM Siddique, F Kratz, S Mahmud and BV Heyst. Energy conversion by nanomaterial-based trapezoidal-shaped leg of thermoelectric generator considering convection heat transfer effect. *J. Energ. Resour. Tech.* 2019, **141**, 082001.
[11] ARM Siddique, K Venkateshwar, S Mahmud and BV Heyst. Performance analysis of bismuth-antimony-telluride-selenium alloy-based trapezoidal-shaped thermoelectric pallet for a cooling application. *Energ. Convers. Manag.* 2020; **222**, 113245.
[12] S Shittu, G Li, X Tang, X Zhao, X Ma and A Badiei. Analysis of thermoelectric geometry in a concentrated photovoltaic-thermoelectric under varying weather conditions. *Energy* 2020; **202**, 117742.
[13] OI Ibeagwu. Modelling and comprehensive analysis of TEGs with diverse variable leg geometry. *Energy* 2019; **180**, 90-106.
[14] AL Khalil, A Elhassnaoui, S Yadir, O Abdellatif, Y Errami and S Sahnoun. Performance comparison of TEGs for diverse variable leg geometry with the same leg volume. *Energy* 2021; **224**, 119967.
[15] Q Doraghi, N Khordehgah, A Zabnienska-Góra, L Ahmad, L Norman, D Ahmad and H Jouhara. Investigation and computational modelling of variable teg leg geometries. *ChemEngineering* 2021; **5**, 45.
[16] AS Al-Merbati, BS Yilbas and AZ Sahin. Thermodynamics and thermal stress analysis of thermoelectric power generator: Influence of pin geometry on device performance. *Appl. Therm. Eng.* 2013; **50**, 683-92.
[17] PE Ruiz-Ortega, MA Olivares-Robles and OYEMD Oca. Segmented thermoelectric generator under variable pulsed heat input power. *Entropy* 2019; **21**, 929.
[18] Z Ye-Qi Zhang, J Sun, W Guang-Xu and W Tian-Hu. Advantage of a thermoelectric generator with hybridization of segmented materials and irregularly variable cross-section design. *Energies* 2022; **15**, 2944.
[19] CA Badillo-Ruiz, MA Olivares-Robles and PE Ruiz-Ortega. Performance of segmented thermoelectric cooler micro-elements with different geometric shapes and temperature-dependent properties. *Entropy* 2018; **20**, 118.
[20] R Kumar, C Maduabuchi, R Lamba, M Vashishtha and S Upadhyaya. Transient optimization of a segmented variable area leg geometry-based solar thermoelectric generator. *In*: Proceedings of the 2021 IEEE Green Energy and Smart Systems Conference (IGESSC), Long Beach, California. 2021.
[21] H Tian, X Sun, Q Jia, X Liang, G Shu and X Wang. Comparison and parameter optimization of a segmented thermoelectric generator by using the high temperature exhaust of a diesel engine. *Energy* 2015; **84**, 121-30.
[22] H Liu, J Meng, X Wang and W Chen. A new design of solar thermoelectric generator with combination of segmented materials and asymmetrical legs. *Energ. Convers. Manag.* 2018; **175**, 11-20.
[23] G Zhang, L Fan, Z Niu, K Jiao, H Diao, Q Du and G Shu. A comprehensive design method for segmented thermoelectric generator. *Energ. Convers. Manag.* 2015; **106**, 510-19.
[24] H Tian, N Jiang, Q Jia, X Sun, G Shu and X Liang. Comparison of segmented and traditional thermoelectric generator for waste heat recovery of diesel engine. *Energ. Procedia* 2015; **75**, 590-6.
[25] Y Ge, Z Liu, H Sun and W Liu. Optimal design of a segmented thermoelectric generator based on three-dimensional numerical simulation and multi-objective genetic algorithm. *Energy* 2018; **147**, 1060-9.
[26] S Shittu, G Li, Q Xuan, X Zhao, X Ma and Y Cui. Electrical and mechanical analysis of a segmented solar thermoelectric generator under non-uniform heat flux. *Energy* 2020; **199**, 117433.
[27] S Shittu, G Li, X Zhao, X Ma, YG Akhlaghi and E Ayodele. High performance and thermal stress analysis of a segmented annular thermoelectric generator. *Energ. Convers. Manag.* 2019; **184**, 180-93.
[28] RO Suzuki, KO Ito and S Oki. Analysis of the performance of thermoelectric modules under concentrated radiation heat flux. *J. Electron. Mater.* 2016; **45**, 1827-35.
[29] JD Angelo, lD Case, N Matchanov, CI Wu, TP Hogan, J Barnard, C Cauchy, T Hendricks and MG Kanatzidis. Electrical, thermal, and mechanical characterization of novel segmented-leg thermoelectric modules. *J. Electron. Mater.* 2011; **40**, 2051-62.
[30] A El-abidi, S Yadir, F Chanaa, M Benhmida, H Amiry, H Bousseta and H Ezzaki. Modeling and simulation of a modified solar air heater destined to drying the gelidium sesquipedale. *Int. J. Renew. Energ. Res.* 2018; **8**, 2003-13.